Available online at www.sciencedirect.com
ScienceDirect
Radiation Measurements 42 (2007) 521–527
Radiation Measurements
www.elsevier.com/locate/radmeas

Single crystalline film scintillators based on Ce- and Pr-doped aluminium garnets

Y. Zorenko[a,*], V. Gorbenko[a], E. Mihokova[b], M. Nikl[b], K. Nejezchleb[c], A. Vedda[d], V. Kolobanov[e], D. Spassky[e]

[a]*Laboratory of Optoelectronic Materials (LOM), Department of Electronic, Ivan Franko National University of Lviv, 79017 Lviv, Ukraine*
[b]*Institute of Physics AS CR, Cukrovarnicka 10, 162 53 Prague, Czech Republic*
[c]*Crytur Ltd., Palackeho 175, 51119 Turnov, Czech Republic*
[d]*Department of Materials Science, University of Milano-Bicocca, via Cozzi 53, 20125 Milano, Italy*
[e]*Physical Faculty, Moscow State University, 119899 Moscow, Russia*

Received 17 December 2006; accepted 31 January 2007

Abstract

Luminescence and scintillation properties of single crystalline films (SCF) of Ce- and Pr-doped $Y_3Al_5O_{12}$ (YAG) and $Lu_3Al_5O_{12}$ (LuAG) garnets were analysed and compared with their bulk single crystal (SC) analogues. It was shown that the main peculiarities of luminescent properties of Ce- and Pr-doped YAG and LuAG SCF are due to the absence of Y_{Al} and Lu_{Al} antisite defects (AD) and to the extremely low concentration of vacancy-type defects in SCF with respect to SC. In SCF the absence of the AD-related traps results in faster energy transfer to the emission centres and accelerated scintillation response.

Keywords: Garnets; Single crystal and single crystalline films; Ce^{3+} and Pr^{3+} impurities; Scintillators; Luminescence; Light yield

1. Introduction

R&D of the phosphors based on single crystalline films (SCF) of Al_2O_3–Y_2O_3–Lu_2O_3 oxide compounds obtained by liquid phase epitaxy (LPE) was the subject of intensive investigations during last years (Zorenko et al., 2005a; Nikl, 2006, and references therein). At present, the fields of applications of SCF as luminescent detectors of ionising radiation include scintillators for monitoring of α- and β-particles and "phosvich"-type scintillators/detectors for registration of the components of mixed ionizing fluxes, screens for visualization of x-ray images with high spatial resolution and screens for electron-beam tubes (Zorenko et al., 2005a). Starting oxide compounds for development of the SCF phosphors are usually Ce^{3+}- and Pr^{3+}-doped SCF of $Y_3Al_5O_{12}$ (YAG) and $Lu_3Al_5O_{12}$ (LuAG) garnets.

The main peculiarities of the luminescent properties of garnets SCF phosphors with respect to single crystal (SC) analogues are the absence of the Y_{Al} and Lu_{Al} antisite defects (AD) (Y and Lu cations localized in octahedral sites of the Al cations) and the extremely low concentration of vacancy-type defects (Zorenko et al., 2004; Zorenko et al., 2005a, b). Unlike SCF, in the SC of YAG and LuAG garnets the content of Y_{Al} and Lu_{Al} AD is about 0.25–0.5 at% (Ashurov et al., 1977; Lupei et al., 1995). The presence of AD is an inevitable consequence of the high melting temperature (about 2000 °C) of the bulk SC grown from the melt by Czochralski or Bridgman methods (Geller et al., 1972; Kuklja, 2000; Stanek et al., 2006). Due to the presence of AD, the bulk SC garnets present a specific type of "self-activated" phosphors where the Y_{Al} and Lu_{Al} AD as analogues of isoelectronic impurities create the emission centres in near-UV region (Zorenko, 2005) and trapping centres (Nikl et al., 2005; Vedda et al., 2006).

It is worth noting that scintillation decays of bulk SC scintillators usually show a noticeable presence of slow components originating from delayed radiative e/h recombination at Ce^{3+} and Pr^{3+} ions, most probably given by their re-trapping at defect-related shallow traps during the transport stage of the

* Corresponding author.
E-mail address: zorenko@electronics.wups.lviv.ua (Y. Zorenko).

1350-4487/$ - see front matter © 2007 Elsevier Ltd. All rights reserved.
doi:10.1016/j.radmeas.2007.01.045

energy transfer (Nikl, 2005). For example, for LuAG:Ce and LuAG:Pr SC scintillators it was determined (Mares et al., 2007) that more than 74 and 58%, respectively, of the light yield (LY) comes from the mentioned delayed recombination processes.

On the contrary, due to the low preparation temperature (850–1100 °C) and the specific crystallization mechanism from melt-solution (MS), the SCF are free from AD and vacancy-type defects (Zorenko et al., 2004). Therefore, one can expect substantially better spectral-kinetic characteristics of scintillators based on Ce- and Pr-doped YAG and LuAG SCF in comparison with their SC analogues.

This work aims in demonstrating the advantages of scintillators based on YAG:Ce and LuAG:Ce SCF with respect to SC. We present a comparative investigation of the luminescence properties of SC and SCF under synchrotron radiation (SR) excitation considering the energy transfer processes from garnet hosts to Ce^{3+} or Pr^{3+} as well. Thermally stimulated luminescence characteristics of Ce-doped Y(Lu)AG SC and SCF are also reported.

2. Samples and experimental technique

Ce- and Pr-doped YAG and LuAG SC were grown by Crytur Ltd. (Czech Republic) from melt by the Bridgman method from a Mo-crucible in reducing atmosphere from the charge containing Y_2O_3, Lu_2O_3, CeO_2 or Pr_2O_3 oxides of 5 N purity and Al_2O_3 oxide of 4 N purity. Ce- and Pr-doped YAG and LuAG SCF were grown by LPE in the LOM of Lviv University (Ukraine) from the MS based on the $PbO–B_2O_3$ flux and crystal-forming oxides of the same purity on the substrates of undoped YAG and LuAG SC (see for details Zorenko and Gorbenko, 2007)

The spectral-kinetic characteristics of Ce- and Pr- doped Y(Lu)AG SC and SCF were investigated at 9 and 300 K (RT) at the Superlumi station (HASYLAB at DESY) under excitation by SR with energy of 3.7–25 eV. The emission and excitation spectra were measured both in the integral regime and in time gates of 1.2–6 and 150–200 ns (fast and slow components, respectively) in the limits of SR pulse with a repetition time of 200 ns and a duration of 0.127 ns. The decay kinetics of luminescence was measured in the 0–200 ns time range at RT. Wavelength-resolved TSL measurements were performed in the 10–310 K range using a CTI closed-cycle refrigerator after X-ray irradiation at 10 K (with a Philips2274 X-ray tube operated at 20 kV), with a homemade apparatus allowing the detection of the TSL signal both as a function of temperature and wavelength in the 280–710 nm interval.

3. Comparative investigation of luminescence of Ce- and Pr-doped YAG and LuAG SC and SCF

3.1. Emission spectra

The emission spectra of YAG:Ce and LuAG:Ce SC(a) and SCF (b) under excitation by SR in the exciton range at 9 K (curves 1) and the region of interband transitions at RT (curves 2) are presented in Figs. 1 and 2, respectively. In the visible range the typical doublet Ce^{3+} $5d^1$–4f luminescence (peaking at 525 and 575 nm for YAG:Ce and 498 and 550 nm for LuAG:Ce) is observed both in SC and SCF under SR

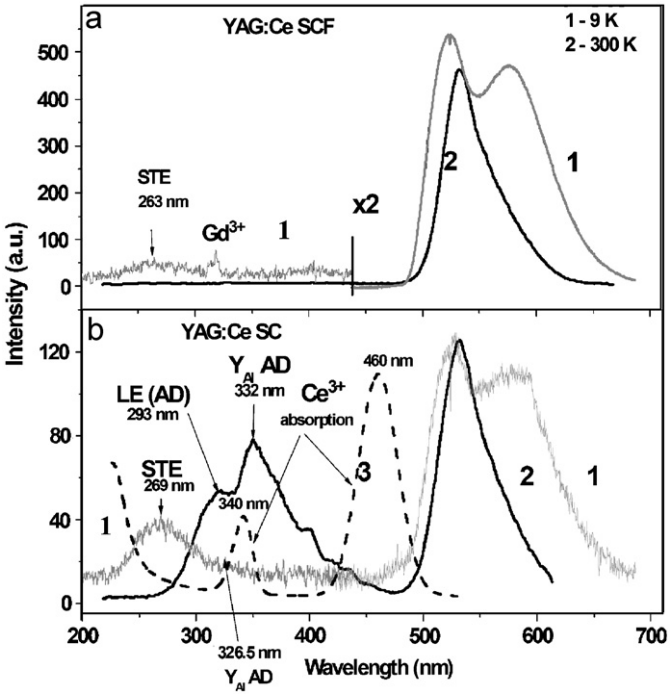

Fig. 1. Luminescence spectra of YAG:Ce SCF (a) and SC (b) at 9 K (1) and RT (2) under excitation by SR with energies of 6.75 eV (2b), 7.3 eV (2a) and 11.3 eV (a, b, curves 1). Absorption spectrum of YAG:Ce SC (b, curve 3) is shown for comparison.

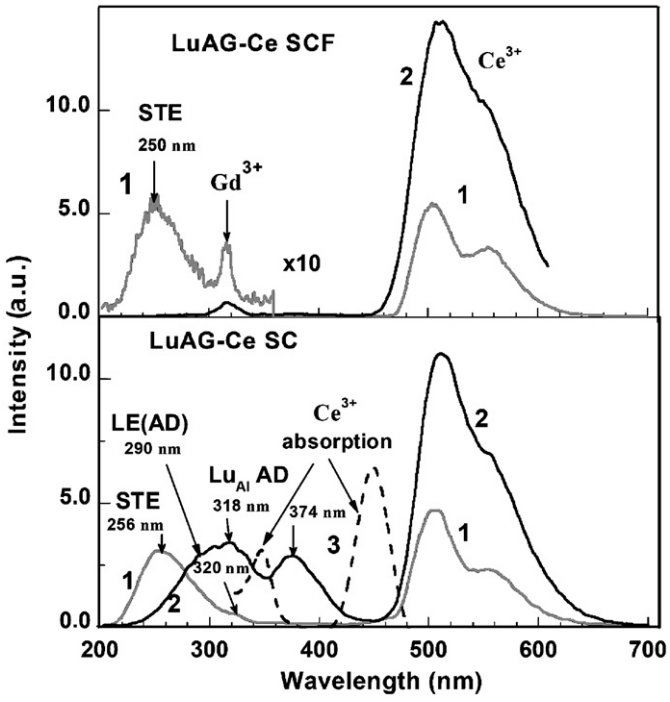

Fig. 2. Luminescence spectra of LuAG:Ce SC (a) and SCF (b) under excitation by SR with an energy of 7.3 eV at 9 K (1) and 7.74 eV at RT (2). Absorption spectrum of LuAG:Ce SC (b, curve 3) is shown for comparison.

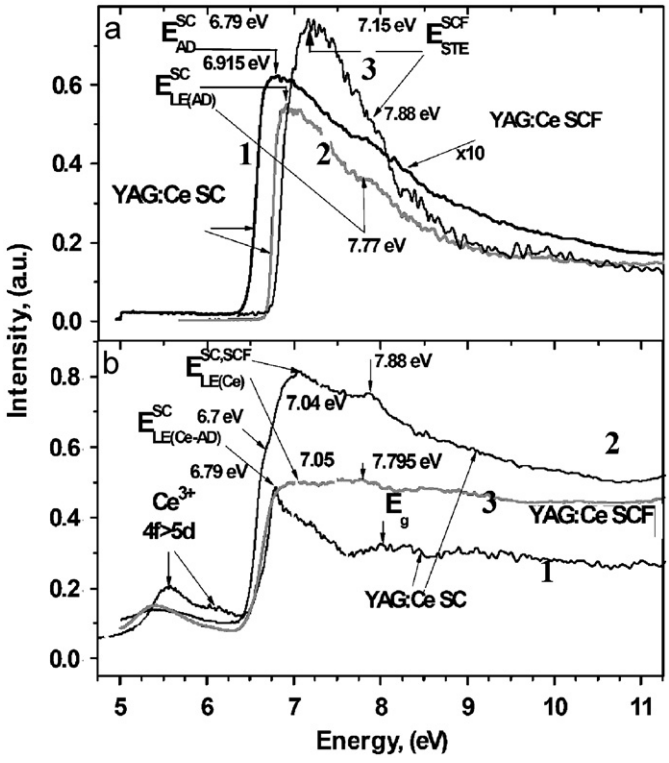

Fig. 3. (a) Excitation spectra of Y_{Al} AD emission at 320 nm at RT (1) and LE (AD) emission at 300 nm at 9 K (2) and the STE emission at 260 nm at 9 K in YAG:Ce SCF (3); (b) excitation spectra of Ce^{3+} ion emission at 530 nm in YAG:Ce SC at 9 K (1) and RT (2) and YAG:Ce SCF at RT (3).

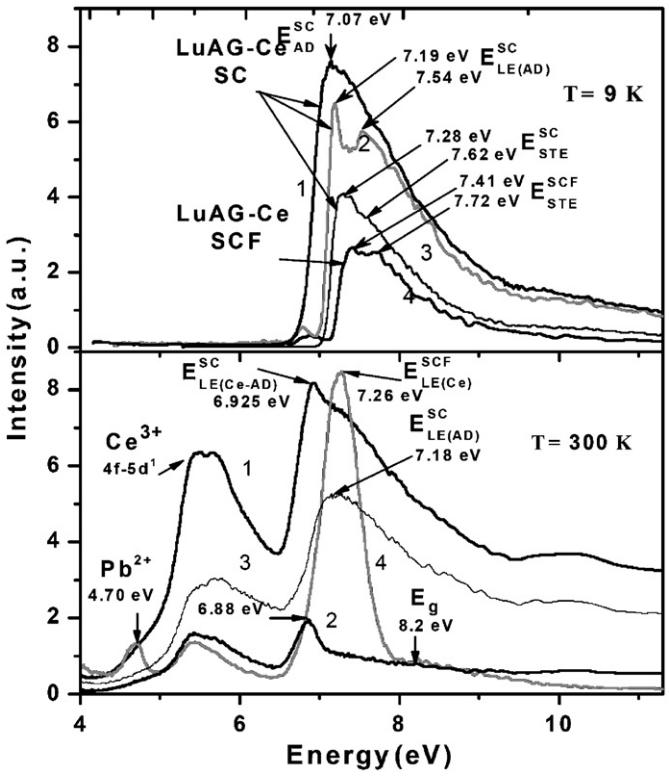

Fig. 4. (a) Excitation spectra of Lu_{Al} AD emission at 325 nm at RT (1), LE (AD) emission at 300 nm (2) and the STE emission at 250 nm at 9 K in the LuAG:Ce SC (3) and SCF (4); (b) excitation spectra of Ce^{3+} emission at 515 nm at RT in LuAG:Ce SC (1–3) and SCF (4) measured in the integral regime (1, 4) and time gates of 1.2–50 ns (2) and 150–200 ns (3) after ending of SR pulse.

excitation with energy of 6.75–7.3 eV. In the UV range the emission spectra of the YAG:Ce and LuAG:Ce SC at 9 K (curves1 in Figs. 2b and 3b, respectively) present the superposition of the bands peaked at 269 and 326.5 nm (YAG) and 256 and 320 nm (LuAG) which are caused, respectively, by the emission of self-trapped excitons (STE) and the Y_{Al} and Lu_{Al} AD (Zorenko et al., 2004). In contrast to SC, only the weak STE emission in the bands peaked at 263 and 250 nm occurs in the luminescence spectra of YAG:Ce and LuAG:Ce SCF in the UV region at 9 K (Figs. 1a and 2a, curves 1, respectively). The sharp peaks at 317 nm in spectra of YAG:Ce and LuAG:Ce SCF are caused by the emission of the Gd^{3+} trace impurity.

Dominating the Y_{Al} and Lu_{Al} AD emission the bands at 332 and 329 nm as well as the emission of excitons localized around the Y_{Al} and Lu_{Al} AD (LE (AD) emission) in the bands at 293 and 290 nm can be seen in the spectra of YAG:Ce and LuAG:Ce SC, respectively, in UV region at RT under excitation by SR in the exciton and interband transition ranges (Figs. 1b and 2b, curves 2). The AD emission bands in YAG:Ce and LuAG:Ce SC are strongly overlapped with the Ce^{3+} ion absorption band at 340 nm (Figs. 1b and 2b, curves3). As a result of this considerable overlap, luminescence of Ce^{3+} ions in YAG:Ce and LuAG:Ce SC is also excited via the AD centres at RT. The LE (AD) and AD emission bands are completely missing in the spectra of YAG:Ce and LuAG:Ce SCF in UV region at RT (Figs. 1a and 2a, curves 2) which confirms the absence of Y_{Al} and Lu_{Al} AD in the SCF of aluminium garnets.

3.2. Excitation spectra of intrinsic emission

The excitation spectra of STE, LE (AD) and AD emission bands in YAG:Ce and LuAG:Ce SC and SCF under excitation by SR in the exciton range are shown in Figs. 3a and 4a, respectively. The emissions at 332 nm (due to Y_{Al}) and at 329 nm (due to Lu_{Al}) at RT are excited in the main bands peaked at 6.79 and 7.07 eV located at the low-energy side of YAG and LuAG SC absorption edges (Figs. 3a and 4a, curves 1, respectively). The excitation spectra of LE (AD) luminescence at 300 nm in YAG:Ce SC at RT and at 290 nm in LuAG:Ce SC at 9 K (Fig. 4a and b, curves 2, respectively) show the fine structure with two peaks at 6.915 and 7.77 eV and 7.20 and 7.55 eV, respectively, which may reflect the existence of two relaxed excited states (RES) of an exciton perturbed or stabilized around the Y_{Al} and Lu_{Al} AD.

The excitation spectra of the STE emission at 260 nm in YAG:Ce SCF (Fig. 3a, curve 3) and at 250 nm in LuAG:Ce SCF (Fig. 4a, curve 4) at 9 K show two peaks at 7.15 and 7.88 eV or at 7.41 and 7.72 eV, respectively, which may be an evidence of the existence of two RES of STE in these garnets. Unlike the SCF, the excitation maxima of the STE emission in LuAG:Ce SC (7.28 and 7.62 eV) are noticeably shifted to the low-energy range with respect to the STE peaks in the SCF probably due to the existence of the excitation bands of LE (AD) emission.

A typical feature of the excitation spectra of YAG:Ce and LuAG:Ce SC is a close spectral location of the main excitation bands of LE (AD) emission at 6.915 eV (at RT) and 7.19 eV (at 9 K) (Figs. 3a and 4a, curves 2, respectively) to the excitation bands of the Y_{Al} and Lu_{Al} AD emission at 6.79 and 7.07 eV (at RT) (Figs. 3a and 4a, curves 1, respectively). Thus, one may conclude that the radiation decay of excitons perturbed by the nearest AD (LE (AD) emission) as well as the AD luminescence predominantly takes place in YAG:Ce and LuAG:Ce SC in the UV region under excitation in the exciton range as distinct to SCF where only weak STE emission occurs in the unperturbed regular sites of garnet lattices.

Table 1
Positions of excitation bands of different centres in Ce- and Pr-doped YAG and LuAG SC and SCF in the exciton range

Type of centre	Positions of excitation bands (eV)			
	YAG SCF	YAG SC	LuAG SCF	LuAG SC
LE (Ce)	7.05[a]	7.04[a]	7.26[a]	6.925[a]
LE (Pr)	7.06		7.34	7.13
Y_{Al} or Lu_{Al} AD	Absent	6.79[a]	Absent	7.07[a]
LE (AD)	Absent	6.92;7.77[a]	Absent	7.19; 7.54
STE	7.15; 7.77		7.41; 7.72	7.28; 7.62
$Ce^{3+} + e + p$	7.795[a]	7.88[a]	8.2[a]	8.2[a]

[a]At 300 K.

3.3. Excitation spectra of Ce^{3+} emission

The excitation spectra of Ce^{3+} luminescence in YAG:Ce and LuAG:Ce SC and SCF are presented in Figs. 3b and 4b, respectively. The fast component of Ce^{3+} emission in LuAG:Ce SC at RT (Fig. 4b, curve 2) and the integral components in YAG:Ce SC at 9 K (Fig. 3b, curve 1) are excited predominantly in the bands at 6.88 and 6.8 eV, respectively. The shape of these bands (narrow intensive line in the region of exciton absorption) is an indication of creation of excitons bound around the Ce^{3+} ions. The excitation bands peaked at 7.88 and 7.795 eV in the spectra of YAG:Ce SC and SCF (Fig. 3a, curves 2 and 3, respectively) and at 8.2 eV in the spectra of LuAG:Ce SC and SCF (Fig. 3a, curves 2 and 4, respectively) on the onset of interband transition of these garnet correspond to the excitation of Ce^{3+} luminescence via recombination of the e/h pair (Zorenko et al., 2005a).

The excitation spectra of integral and slow components of Ce^{3+} emission in LuAG:Ce SC at RT (Fig. 4b, curves 1 and 3, respectively) also consists of the intensive bands at 7.18 eV close to the position of excitation bands of the LE (AD) (7.19 eV) and Lu_{Al} AD (7.07 eV) emission (Fig. 4b, curves 1 and 3, respectively). The excitation spectra of integral components of Ce^{3+} emission in YAG:Ce SC at RT (Fig. 3b, curve 2) also present an additional bump at 6.7 eV close to the position of the excitation band of Y_{Al} AD luminescence (6.79 eV). It evidences an energy transfer to Ce^{3+} ions via the LE (AD) and AD emission centres in YAG:Ce and LuAG:Ce SC (Zorenko et al., 2005a, b).

At the same time, excitation bands of the LE (AD) and Y_{Al} and Lu_{Al} AD luminescence in YAG:Ce and LuAG:Ce SC, respectively, are not present in the excitation spectra of YAG:Ce and LuAG:Ce SCF at RT (Figs. 3b and 4b, curves 3 and 4, respectively). At 9 K the excitation maxima of both fast (7.41 eV) and slow (7.74 eV) components of the Ce^{3+} emission in LuAG:Ce SCF (not shown in Fig. 4a) practically coincide with the excitation maxima of the STE emission (Fig. 4a, curve 4). This indicates that the Ce^{3+} emission in YAG:Ce and LuAG:Ce SCF can be excited mainly through the creation of bound exciton states contrary to SC, where the energy transfer via AD excitation is very significant. Existence of two excitation maxima of the Ce^{3+} emission in LuAG:Ce SCF provides an indication that the RES of an exciton bound around Ce^{3+} ions has two radiative levels (Zorenko et al., 2005b).

Thus, from the data shown in Figs. 3b and 4b we conclude that the spectral location of the excitation maxima of the Ce^{3+} emission for SC are, as a rule, close to the position of excitation bands of the LE (AD) and AD luminescence; i.e., the Y_{Al} and Lu_{Al} AD are significantly involved in the processes of excitation of Ce^{3+} emission in YAG:Ce and LuAG:Ce SC. We can also assume that in Ce-doped YAG and LuAG SC the formation of Ce^{3+}–AD "coupled-centres" takes place with probable non-radiative energy transfer in the case when both centres are sufficiently (< 10 Å) close. Latter condition may happen in YAG:Ce and LuAG:Ce SC due to high Ce^{3+} (0.1–0.25 at%) and AD (0.25–0.5 at%) concentrations. This conclusion is strongly supported by the substantial difference in the spectral location of the excitation maxima of an exciton bound around Ce^{3+} ion in LuAG:Ce SC (6.88 eV) and SCF (7.26 eV) as well as by the difference in the shape of the excitation spectra for SC and SCF in the exciton range (Fig. 4b, curves 1 and 4, respectively).

Positions of all excitation bands of the Ce^{3+} and Pr^{3+} emission in YAG and LuAG SC and SCF are summarised in Table 1. The notable difference in the positions of excitation bands of Pr^{3+} emission also takes place in the spectra of the LuAG:Pr SC and SCF (Table 1). Apart from the bands noted in Table 1, the excitation spectra of Ce^{3+}emission in the LuAG:Ce SCF also contain the band at 4.70 eV which coincides well with the absorption band caused by the $^1S_0 \rightarrow {}^3P_1$ transition of Pb^{2+} trace impurity (Fig. 4b, curve 4). This makes the energy transfer from Pb^{2+} to Ce^{3+} ions feasible (see in detail in Babin et al., 2007).

3.4. Decay kinetics

Significant difference in the energy transfer from the host to activator ions in SC and SCF is confirmed by the decay kinetics of the Ce^{3+} and AD luminescence in YAG:Ce and LuAG:Ce SC and SCF (Figs. 5 and 6) under the excitation within the 4f > 5d absorption band of Ce^{3+} ions at 3.7 eV (curve 1) and region of interband transitions (10.5–17.7 eV) (curves 2 and 3). The decay kinetics of the Ce^{3+} emission in YAG:Ce and LuAG:Ce SC and SCF at RT under excitation in the band at 3.7 eV is very similar with lifetimes of 66.5 and 51.3 ns,

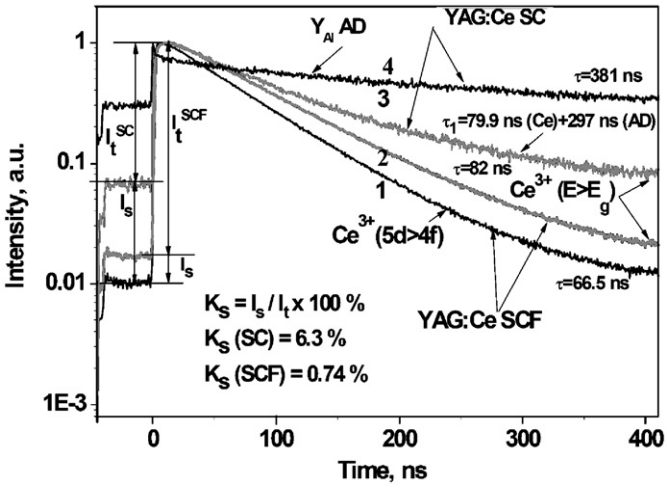

Fig. 5. Decay kinetics Ce^{3+} ion (1–3) emission in the band at 530 nm in YAG:Ce SCF (1, 2) and SC (3) at RT under excitation by SR with energies of 3.7 eV (1) and 10.5 eV (2,3). Curve 4—decay kinetics of Y_{Al} AD emission in the band at 320 nm in YAG SC.

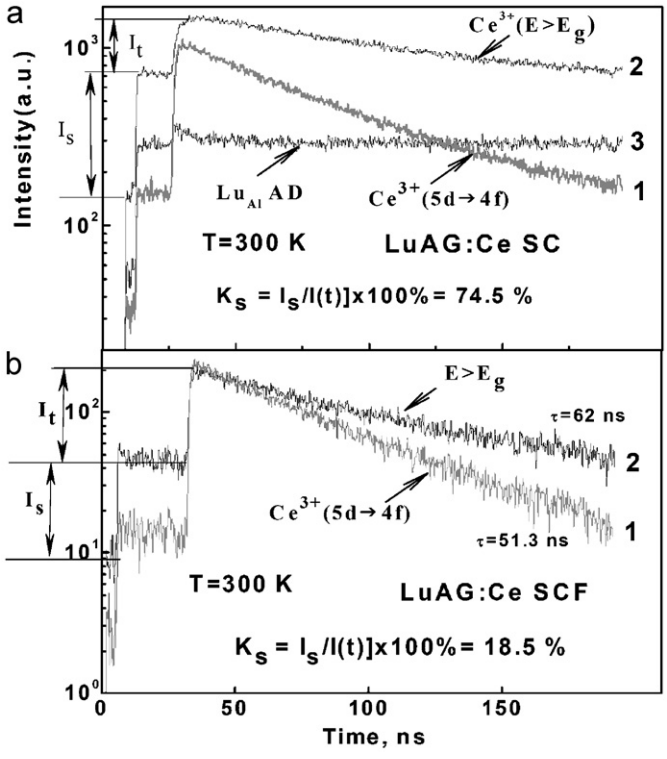

Fig. 6. Decay kinetics of Ce^{3+} ion luminescence in the band at 515 nm in LuAG:Ce SC (a) and SCF (b) of LuAG:Ce at RT under excitation by SR with energies 3.7 eV (1a, b) and 17.2 eV (2a, b). Curve 3a—decay kinetics of Lu_{Al} AD luminescence in the band at 325 nm under excitation by SR with energy of 7.07 eV at RT.

respectively (Figs. 5 and 6a, curves 1). Meanwhile, under interband excitation the decay kinetics of YAG:Ce and LuAG:Ce SC slow down (Figs. 5 and 6b, curves 2). For example, two-exponential fit of emission decay for LuAG:Ce SC (Fig. 6a, curve 2), $I(t) = 152 + 400\exp[-t/(62.5\,\text{ns})] + 905\exp[-t/(288\,\text{ns})]$, points to the substantial (up to 78% of the initial amplitude) contribution of the slow components with $\tau = 288$ ns. A similar approximation (Fig. 5, curve 3) for YAG:Ce SC, $I(t) = 0.04 + 0.82\exp[-t/(79.9\,\text{ns})] + 0.14\exp[-t/(297\,\text{ns})]$, also shows large contribution of slow component with $\tau = 297$ ns.

Table 2
Comparison of the content of slow components for Ce- and Pr-doped YAG and LuAG SC and SCF

Scintillators	Content of slow components, K_s (%)
LuAG:Ce SC	74.5
LuAG:Ce SCF	18.5
YAG:Ce SC	6.3
YAG:Ce SCF	0.74
LuAG:Pr SC	18.2
LuAG:Pr SCF	32.5

To estimate the content of slow components in the scintillation decay we used the ratio between the intensity I_s of decay components which are slower than the repetition frequency of SR and the decay amplitude I_t of rising part of scintillation pulse as $K_s = [I_s/I_t] * 100\%$ (Figs. 5 and 6). For LuAG:Ce SC very high value of $K_s = 74.5\%$ was obtained (Fig. 6a) under excitation with energy of 17.2 eV (Table 2). For LuAG:Pr SC the content of slow component is reduced to 18.2% in comparison with LuAG:Ce SC (Table 2) mainly due to less overlapping of the 4f–5d absorption bands of Pr^{3+} ion at 240 and 280 nm and AD-related emission bands.

In YAG:Ce SCF substantially lower value of $K_s = 6.3\%$ was obtained (Table 2), which reflects relatively small influence of AD in YAG:Ce SCF. For LuAG:Pr SCF the larger content of slow component (32.5%) in comparison with YAG:Ce SCF (Table 2) probably is caused by the significantly larger Pb^{2+} trace impurity influence on the emission of Pr^{3+} ions in the UV range than Ce^{3+} emission in the visible region.

Possible reasons for the presence of slow components in the Ce^{3+} luminescence in YAG:Ce and LuAG:Ce SC are as follows: (i) the existence of the intensive Y_{Al} and Lu_{Al} AD luminescence in UV range in the bands peaked at 329 and 332 nm with the lifetimes of main components of 380 and 540 ns, respectively (determined from the two-exponential fitting of curve 4 in Fig. 5 and curve 3 in Fig. 6a); (ii) the spectral overlap of the Y_{Al} and Lu_{Al} AD emissions with the 4f–5d absorption band of Ce^{3+} ion at 340 nm (Figs. 1a and 2a, curves 3), which enables the re-absorption of AD emission by the Ce^{3+} ions or even non-radiative energy transfer; (iii) re-trapping of free charge carriers mainly at the Y_{Al} and Lu_{Al} AD-based trapping centres under the interband excitation (Nikl et al., 2005; Vedda et al., 2006). In the latter case, a 0.29 eV trap depth was calculated for the Lu_{Al} AD-associated TSL peak at 145 K in LuAG:Ce SC (Fig. 7b), while a lower (0.18 eV) trap depth was evaluated for the TSL peak at 92 K related to Y_{Al} AD in YAG:Ce SC (Fig. 7a) (Nikl et al., 2005). Deeper AD-associated traps and higher AD concentration in LuAG:Ce can explain the higher content of slow decay components with respect to YAG:Ce SC, which was evaluated with the help of the above-mentioned K_s coefficient.

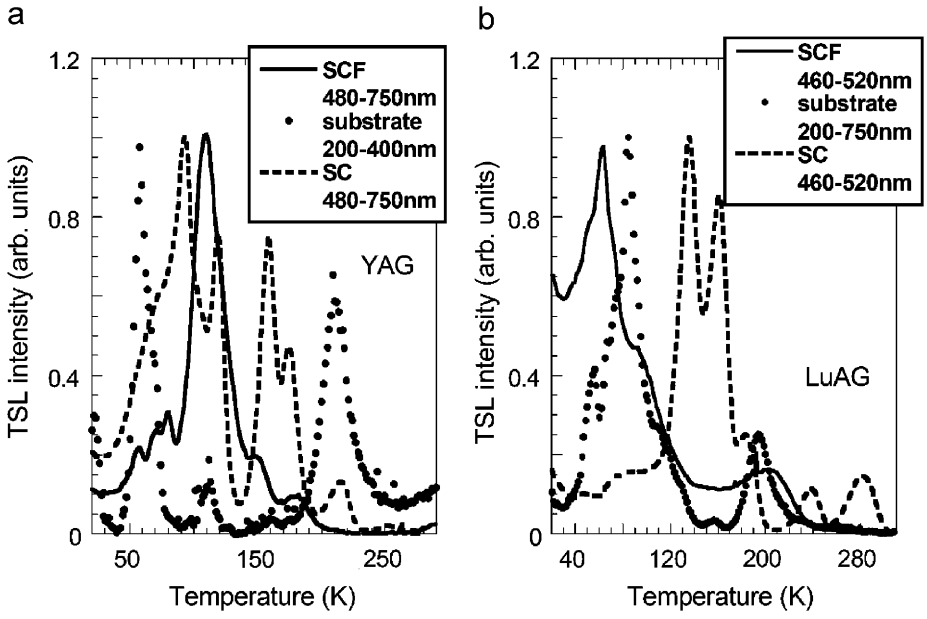

Fig. 7. TSL glow curves of YAG:Ce- (a) and LuAG:Ce-based (b) SC and SCF systems, including their substrates in the case of SCF. Glow curves obtained after integration of wavelength-resolved measurements in the wavelength intervals reported in the legends.

Spectrally resolved TSL measurements of Ce-doped YAG and LuAG SCF do not show the 92 and 145 K peaks, respectively (Fig. 7a and b), further supporting the absence of AD in SCF. In addition, the lower TSL emission intensity in SCF above 150 K indicates a lower concentration of deeper traps associated e.g. with oxygen vacancies.

4. Conclusions

Scintillation properties of YAG:Ce and LuAG:Ce SC scintillators are strongly influenced by the presence of the Y_{Al} and Lu_{Al} AD, which give rise to the new luminescence bands in the UV range and the trapping centres as well. Due to high concentration of both the Ce and AD centres in YAG and LuAG SC the formation of Ce–AD coupled-centres is not excluded, in which a non-radiative energy transfer can take place between the Ce^{3+} ions and Y_{Al} and Lu_{Al} AD. Higher content of slow decay components in LY and scintillation decay of LuAG:Ce SC as compared with YAG:Ce SC are due to larger concentration of AD (0.5 and $\sim$ 0.25 at%, respectively) and more pronounced depth (0.29 and 0.18 eV, respectively) of the AD-related trapping centres.

YAG:Ce and LuAG:Ce SCF scintillators possess better spectral-kinetic properties in comparison with the SC analogues due to the absence of additional channels of dissipation of excitation energy connected with the Y_{Al} and Lu_{Al} AD and vacancy-type defects. The YAG:Ce and LuAG:Ce SCF with respect to the bulk SC show simpler and faster decay kinetics and lower content of slow components of Ce^{3+} luminescence under excitation in the region of interband transitions.

Acknowledgements

The authors express their gratitude to Prof. Dr. G. Zimmerer for his assistance in carrying out the experiments in HASYLAB at DESY. The work was supported by STCU (project 2042) and INTAS (project 04-78-7083) and Czech GACR project No. 202/05/2471.

References

Ashurov, M., Voronko, Yu., Osiko, V., Solol, A., 1977. Spectroscopic investigation of structural disordering of garnet crystals with rare-earth dopants. Phys. Status Solidi A 42, 101–110.

Babin, V., Gorbenko, V., Makhov, A., Nikl, M., Zazubovich, S., Zorenko, Y., 2007. The role of Pb^{2+} ions in the luminescence of LuAG:Ce single crystalline films. Phys. Status Solidi C 4, 797–800.

Geller, S., Espinosa, J.P., Fullmer, L.D., Grandall, P.B., 1972. Thermal expansion of some garnets. Mater. Res. Bull. 7, 1219–1224.

Kuklja, M.M., 2000. Defects in yttrium aluminium perovskite and garnet crystals: atomistic study. J. Phys. Condens. Matter 12, 2953–2967.

Lupei, V., Lupei, A., Tiseanu, C., Georgescu, S., Stoicescu, C., Nanan, P.M., 1995. High-resolution optical spectroscopy of YAG: Nd: a test for structural and distribution models. Phys. Rev. B 51, 8–17.

Mares, J.A., Beitlerova, A., Nikl, M., Wedda, A., D'Ambrosio, C., Blazek, K., Nejezchleb, K., 2007. Time development of scintillating response in Ce- or Pr-doped crystals. Phys. Status Solidi C 4, 996–999.

Nikl, M., 2005. Energy transfer in the luminescence of wide band-gap scintillators. Phys. Status Solidi A 202, 201–206.

Nikl, M., 2006. Scintillation detectors for X-rays. Meas. Sci. Technol. 17, R37–R54.

Nikl, M., Mihokova, E., Pejchal, J., Vedda, A., Zorenko, Yu., 2005. The antisite Lu_{Al} defect-related trap in $Lu_3Al_5O_{12}$:Ce single crystal. Phys. Status Solidi B 242, R119–R121.

Stanek, C.R., McClellan, K.J., Levy, M.R., Grimes, R.W, 2006. Extrinsic defect structure of $RE_3Al_5O_{12}$ garnets. Phys. Status Solidi B 243, R75–R77.

Vedda, A., Fassoli, M., Moretti, F., Mihokova, E., Nikl, M., Pejchal, J., Zorenko, Yu., Gorbenko, V., Blazek, K., Nejezchleb, K., 2006. Trap levels

and recombination centers in LPE grown Ce-doped LuAG and YAG thin films. in: Gektin, A., Grinyov, B. (Eds.), Proceedings of SCINT 2006, pp. 464-467.

Zorenko, Y., 2005. Luminescence of isoelectronic impurities and anti-site defects in garnets. Phys. Status Solidi C 26, 375–379.

Zorenko, Y., Voloshinovskii, A., Konstankevych, I., Kolobanov, V., Mikhailin, V., Spassky, D., 2004. Luminescence of excitons and antisite defects in the phosphors based on garnet compounds. Radiat. Meas. 38, 677–680.

Zorenko, Y., Gorbenko, V., Konstankevych, I., Voloshinovskii, A., Stryganyuk, G., Mikhailin, V., Kolobanov, V., Spassky, D., 2005a. Single-crystalline films of Ce-doped YAG and LuAG phosphors: advantages over bulk crystals analogues. J. Lumin. 114, 85–94.

Zorenko, Yu., Gorbenko, V., Voloshinovskii, A., Stryganyuk, G., Mikhailin, V., Kolobanov, V., Spassky, D., Nikl, M., Blazek, K., 2005b. Exciton-related luminescence in LuAG:Ce single crystals and single crystalline films. Phys. Status Solidi A 202, 1113–1118.

Zorenko, Y., Gorbenko, V., 2007. Growth peculiarities of the $R_3Al_5O_{12}$ (R = Lu, Yb, Tb, Eu-Y) single crystalline film phosphors by liquid phase epitaxy. Radiat. Meas., this issue, doi: 10.1016/j.radmeas.2007.02.049.